

The mesospheric inversion layer and sprites

S. Fadnavis¹, Devendraa Siingh^{1*}, R.P. Singh²

¹Indian Institute of Tropical Meteorology, Pune-411 008, India.

²Vice-Chancellor, Veer Kunwar Singh University, Ara (Bihar)-802301, India.

* also at, Center for Sun-Climate Research, Danish National Space Center, DK-2100,
Copenhagen, Denmark

Abstract

The vertical structure of temperature observed by SABER (Sounding of Atmosphere using Broadband Emission Radiometry) aboard TIMED (Thermosphere, Ionosphere, Mesosphere Energetics and Dynamics) and sprites observations made during the Eurosprite 2003-2007 observational campaign were analyzed. Sprite observations were made at two locations in France, namely Puy de Dôme (45° 46' 19.2''N; 02° 57' 44.64''E; 1.464 km altitude) in the French Massif Central and at the Pic du Midi (42° 56' 11''N; 00° 08' 34''E; 2.877 km altitude) in the French Pyrénées. It is observed that the vertical structure of temperature shows evidence for a Mesospheric Inversion Layer (MIL) on those days on which sprites were observed. A few events are also reported in which sprites were not recorded, although there is evidence of a MIL in the vertical structure of the temperature. It is proposed that breaking gravity waves produced by convective thunderstorms facilitate the production of (a) sprites by modulating the neutral air-density and (b) MILs via the deposition of energy. The same proposition has been used to explain observations of lightnings as well as both MILs and lightning arising out of deep convections.

23 **1. Introduction**

24 Mesospheric Inversion Layers (MILs) over low and mid-latitudes have been reported
25 in a number of studies [*Schmidlin, 1976; Hauchecorne et al., 1987; Leblanc and*
26 *Hauchecorne, 1997; Meriwether et al., 1998; States and Gardner, 1998; Kumar et al., 2001;*
27 *Fadnavis and Beig, 2004; Fadnavis et al., 2007*]. There are two types of MILs (1) lower
28 MILs (~75km) and (2) upper MILs (~90 km) [*Fadnavis and Beig, 2004; Meriwether and*
29 *Gerrard, 2004*]. Possible mechanisms for production of MILs have been reviewed by
30 [*Meriwether and Gardner, 2000*]. *Meriwether and Gerrard [2004]* stated that the lower MILs
31 are the result of dissipating planetary waves and a mechanism responsible for the formation
32 of the upper MIL may be nonlinear gravity wave-tidal interactions. In some studies [*States*
33 *and Gardner, 1998; Chu et al., 2005*] the upper MIL is attributed to the diurnal tides, whereas
34 others [*Meriwether et al., 1998; Liu and Hagan, 1998; Liu et al., 2000; Oberheide et al.,*
35 *2006*] proposed the coupling of gravity waves (GWs) and the mesopause tidal structures to
36 produce the upper MILs. *Thomas et al. [1996], Gardner and Yang [1998]* and *Meriwether et*
37 *al. [1998]* indicated that GW breaking plays an important role in the development of the
38 upper MIL. Two-dimensional modeling studies reveal that GWs play a significant role in
39 increasing the temperature amplitude of the tidal structure and thus contribute to MIL
40 [*Hauchecorne and Maillard, 1990; Leblanc et al., 1995*].

41 Gravity waves are produced by oscillating updrafts and downdrafts in convective
42 systems [*Fovell and Ogura, 1989*]. The excited gravity wave amplitudes are proportional to
43 the convective core updraft velocity, stronger updrafts lead to large-amplitude-gravity waves.
44 Gravity waves propagating upward into the high atmosphere may amplify and become a
45 major source of mechanical energy and momentum into this region from below [*Swenson and*
46 *Liu, 1998*]. Breaking gravity waves modulate neutral density in the mesosphere: reduced
47 density values will facilitate the electrical breakdown process [*Sao Sabbas et al., 2009*]. This

48 concept has been used to explain modulated optical emissions in the nightglow layer, which
49 are detectable from the ground [*Taylor and Hill, 1991; Turnbull and Lowe, 1991*] as well as
50 from orbiting imaging platforms [*Dewan et al., 1998; Picard et al., 1998*]. *Sentman et al.*
51 [2003] documented the first complete ring structure of OH emissions modulated by
52 thunderstorms. Their analysis revealed that short period concentric wave structures emanated
53 radially outward from a central excitation region directly above the storm whose period
54 gradually increases and wave length decreases with time.

55 Sprites are luminous events observed in the mesosphere in association with lightning
56 ground flashes of positive polarity [*Boccippio et al., 1995; Singh et al., 2004; Siingh et al.,*
57 *2005; Siingh et al., 2007 with reference therein*]. Several mechanisms based on the
58 relationship between positive electrical charges in the troposphere and a physical process in
59 the mesosphere is proposed for the production of sprites. The physical processes include
60 sprite production by electrical breakdown [*Wilson, 1925; Huang et al. 1999*], electrical
61 heating [*Pasko et al., 1995*], electron runaway [*Bell et. al., 1995*], runaway electron beams
62 [*Roussel-Dupre and Gurevich, 1996; Lehtinen et al., 1997*], high altitude gamma rays
63 [*Taranenko and Roussel-Dupre, 1996*] and infrared glow from CO₂ emission [*Picard et al.,*
64 *1997*]. A few cases of sprites induced by negative cloud-to-ground flashes have also been
65 reported [*Barrington-Leigh et. al., 1999*] as discussed in *Williams et al.* [2007], who
66 investigated the origins of the pronounced polarity asymmetry for sprites. *Williams* [1998]
67 reviewed the atmospheric electrical and meteorological observations and proposed that
68 sprites are produced by laterally extensive mesoscale convective systems (MCSs) in which
69 the positive charge reservoir predominates in the 4-6 km of altitude. MCSs are characterized
70 by laterally extensive regions of stratiform precipitation with a total area larger than 10⁴ km²,
71 which is usually more than an order of magnitude greater than the area of ordinary
72 thunderstorms. It is also suggested that sprites are associated with “spider lightning” which is

73 extended horizontal lightning in clouds that may feed several CG flashes [*Mazur et al.*,
74 1998]. Recently *Soula et al.* [2009a] analyzed two storms, each producing 27 sprite events
75 observed during the EuroSprite campaigns. Both storms were identified as MCSs with a
76 trailing stratiform configuration and reaching a maximum cloud area of $\sim 12 \times 10^4 \text{ km}^2$.

77 Sprites may affect the ionization of the mesosphere which can be estimated from the
78 observations of amplitude perturbations of VLF waves propagating through it. Based on
79 EuroSprite-2003 observations, *Mika et al.* [2005] had suggested that sprites are nearly always
80 accompanied by “early” VLF perturbations having long recovery times ($\sim 30\text{--}300\text{s}$); which
81 suggests spatially extended, diffuse regions of electron density increases at altitudes higher
82 than 75 km [*Neubert et al.*, 2008]. This supports theoretical predictions of air breakdown in
83 the upper D-region ionosphere during sprite occurrences, triggered by strong quasi-
84 electrostatic (QE) fields [*Wilson*, 1925]. Another category of VLF perturbations with a long
85 onset duration of up to 2.5s was observed in relation to $\sim 55\%$ of the sprite events as discussed
86 by *Neubert et al.* [2008]. They have suggested that the long onset duration is a result of
87 secondary ionization build-up in and/or heating of the upper D-region below the nighttime
88 VLF reflection height, caused by electromagnetic pulses radiated upwards from horizontal
89 intra-cloud discharges. The radiation fields accelerate sprite-produced electrons which then
90 impact to produce secondary electrons in an avalanche process leading to ionization build-up
91 [*Haldoupis et al.*, 2006]. The enhancement in electrical conductivity of mesosphere during
92 sprite was supported by *Williams et al.* [2006] based on “glow discharge tube”
93 measurements, who observed electrical conductivity $\sim 3 \times 10^{-5} \text{ S/m}$ for a radiance value in the
94 range of sprite measurement. This value is some three orders of magnitude greater than the
95 ambient electrical conductivity at the simulated altitude ($\sim 65\text{km}$).

96 Sprites may also produce NO_x in the stratosphere [*Sentmen et al.*, 2008; *Enell et al.*,
97 2008; *Neubert et al.*, 2008; *Siingh et al.*, 2008]. The production may involve excitation of N_2

98 into short-lived states which cascade into the metastable N_2 ($A^3\Sigma_u^+$) state, ionization of N_2
99 and O_2 , and dissociation of O_2 [Enell et al., 2008]. In regard to NO_x production, the Sentman
100 et al. [2008] study showed that the principal reactions leading to production of NO_x were
101 dissociation of N_2 in the head of a sprite-streamer leading to creation of active atomic
102 nitrogen N (2D), which then interacts with O_2 to produce NO. Enell et al. [2008] estimated
103 the total production of NO_x to be around five times the background in the streamers, whereas
104 the model of Gorodillio-Vajquez [2008] predicts NO and NO_x enhancements of a factor of
105 10. Neubert et al. [2008] estimated the total number of NO molecules produced in a streamer
106 $\sim 1.5 \times 10^{19}$, with an estimated average total production on the order of 10^{23} – 10^{25} molecules
107 per streamer. Considering the global occurrence rate of sprites to be 3/min., the total global
108 production of $NO_x \sim 10^{31}$ molecules per year [Neubert et al., 2008; Sentman et al., 2008],
109 which on global scale is quite small [Neubert et al., 2008, Siingh et al., 2008]. The local
110 enhancements of sprite-induced NO_x increases with altitude from a few percent at 47 km to
111 tens of percent at 60 km [Neubert et al., 2008], thus being roughly consistent with Sodankyla
112 Coupled Ion-neutral Chemistry (SIC) model estimates [Enell et al., 2008]. Data from the
113 Global Ozone Monitoring by Occultation of Stars (GOMOS) instrument on ENVIRONMENTAL
114 SATellite (ENVISAT) did not support enhancements on larger regional scales [Rodger et al.,
115 2008]. The enhancement in NO_x concentration decreases ozone concentration through
116 catalytic cycles. The impact of the sprite-produced NO on ozone was estimated to decrease
117 the ozone concentration by a few percent in the 50-60 km altitude range [Enell et al., 2008].
118 Thus, significant ozone perturbations from sprites are unlikely, except for sprite-active
119 storms.

120 Recently Fadnavis et al. [2007] have analyzed the vertical profiles of temperature, the
121 mesospheric ozone volume mixing ratio and the thunderstorm occurrence rate for the same
122 period and studied the possible relationships between thunderstorms and the mesospheric

123 heating near 70-85 km altitude. They showed a fairly good correlation (correlation coefficient
124 lies between 0.50 and 0.72) between the inversion days (days on which MIL was observed in
125 temperature profile) and thunderstorm activity. They have also reported some inversion days
126 on which thunderstorms were not recorded at the corresponding station. The seasonal
127 variation of frequency of the occurrence and the amplitude of the inversion also exhibits a
128 fairly good correlation (correlation coefficient > 0.5) with the seasonal variation of ozone
129 concentration over these regions. *Fadnavis et al.* [2007] considered that gravity waves
130 produced during convective thunderstorms propagating upwards become unstable in the
131 mesosphere and that gravity waves break there [*Thomas et al.*, 1996]. The turbulent heating,
132 arising from the breaking of waves, provides a feedback mechanism that then may maintain
133 the observed MIL [*Wu and Killeen*, 1996; *Fadnavis et al.*, 2007]. Exothermic chemical
134 reactions involving ozone also produce heating [*Mlynczak and Solomn*, 1993], which may
135 add to gravity wave heating. This may explain the positive correlation between thunderstorms
136 and MILs.

137 Figure 1 shows the location of blue jets, red sprites and elves with height. In the same
138 figure, the variation of temperature and occurrence of mesospheric inversion along; with the
139 demarcation of the troposphere, stratosphere, mesosphere and thermosphere are also given
140 [*Lyons et al.*, 2000, *Neubert*, 2003, modified figure]. Sprites and the mesospheric inversion
141 layer occur at the same height in the atmosphere. An attempt is made to understand the
142 relationship between sprites and MIL through a physical mechanism involving gravity waves.

143 **2. Data and Analysis**

144 The Sounding of the Atmosphere using Broadband Emission Radiometry (SABER)
145 instrument is one of four instruments mounted on the Thermosphere Ionosphere Mesosphere
146 Energetics and Dynamics (TIMED) satellite [*Christensen et al.*, 2004]. It was launched in
147 December 2001 into a 625 km orbit inclined at 74 degrees to the equator. The TIMED

148 satellite orbits the Earth about 15 times per day, and measures approximately 100 vertical
149 profiles of temperature on each orbit. SABER has a vertical resolution of about 2 km in the
150 altitude range 10–105 km, and an along-track resolution of approximately 400 km. It is used
151 to study the mesosphere and lower thermosphere/ionosphere region of the Earth's
152 atmosphere. It is a 10-channel infrared (1.27 to 17 μ m) radiometer that observes atmospheric
153 emissions from the Earth's limb. The collected data are ground-processed to retrieve
154 temperature, ozone, water vapor, carbon dioxide, and key parameters describing the
155 energetics of the high atmosphere. Kinetic temperatures are determined from 15 μ m CO₂
156 emissions, taking account of the non-LTE (non local thermodynamic equilibrium) conditions
157 in the MLT region, in combination with 4.3 μ m CO₂ emission used to derive the CO₂ volume
158 mixing ratio [Mertens *et al.*, 2004]. Preliminary estimates of temperature error are quoted as
159 5K for the systematic error and 2K for the accuracy at 87 km.

160 The temperature measurements are continuously available from January 2002 at the
161 website: <http://saber.gats-inc.com/index.php>. The SABER (Level 2A) temperature results for
162 the period 2003 to 2007 are used for this study. The daily temperature profiles from 50 km to
163 100 km show the most notable feature “inversion” in the temperature structure of
164 mesosphere. The days on which the vertical profile of temperature shows a MIL are known as
165 inversion days and the other days are known as non-inversion days (Figure 2). The MILs of
166 amplitude 10 K or more can be considered as significant [Meriwether and Gerrard, 2004,
167 Fadnavis and Beig 2004; Fadnavis *et al.*, 2007]. The MILs are found as a layer ~10-15 km
168 vertical thickness within the upper mesosphere at the equatorial and mid-latitude regions
169 [Meriwether and Gerrard, 2004]. Hence small perturbations (near 80 km) with rise in
170 temperature less than 10K and vertical thickness less than 10km in vertical profile of
171 temperature, as seen in figure 3 are not considered as MILs.

172 To understand the relationship between mesospheric inversion layers and sprites,
173 observations of sprites during the EuroSprite (2003-2007) campaign were analyzed along
174 with the SABER temperature profiles. The sprite observations were made at two locations in
175 France, namely Puy de Dôme (45° 46' 19.2''N; 02° 57' 44.64''E; 1.464 km altitude) (in the
176 French Massif Central) and Pic du Midi (42° 56' 11''N; 00° 08' 34''E; 2.877 km altitude) (in
177 the French Pyrénées) [Chanrion *et al.*, 2007; Neubert *et al.*, 2008]. Sprites were detected for
178 the period 2003-2007 in the months of July-August-September-October. Transient luminous
179 events were detected above MCSs using ground-based observing facilities during four years
180 “Coupling of Atmospheric Layers (CAL)” observations [Neubert *et al.*, 2008]. Vertical
181 temperature profiles obtained from SABER instrument, approximately above (20 to 140 km
182 altitude and $3^0 \times 3^0$ grid) the Puy de Dôme and Pic du Midi locations are analyzed.

183 During the Eurosprite campaigns thunderstorms were monitored with a more
184 complete set of instrumentation, thereby allowing a better characterization of cloud and
185 lightning properties of the sprite-producing regions of the storms. The details about the
186 experiments of these stations and other information with camera details have been discussed
187 by Chanrion *et al.* [2007], Neubert *et al.* [2008] and Sao Sabbas *et al.* [2009]. Short range
188 lightning detection system SAFIR were located in northern Spain and in the Provence region
189 of Southern France. Each has three VHF (~ 100 MHz) receivers in a triangle with ~ 100 km
190 distance between the receivers that measure activity in clouds, giving information on the
191 location (in the horizontal plane) and time of IC (intra-cloud) and CG (cloud-to-ground)
192 flashes (Dru`e *et al.*, 2007). Additional information came from a broad-band, VLF (~ 10
193 kHz) receiver located at Nancay. CG activity was also available from conventional lightning
194 detection networks provided by the French Météorage system of 17 sensors covering the
195 whole country. Each sensor uses two techniques for CG location by direction finding (DF)

196 and time of arrival (TOA). The characteristics of the CG flashes include the location
197 (horizontal), the time of occurrence, the polarity, the multiplicity and the peak currents of
198 each stroke [Cummins *et al.* 1998]. Other characteristics of thunderstorms are derived from
199 meteorological radars. A network of weather radars, ARAMIS, run by MeteoFrance, covers
200 France. Eighteen radars (ten C-band and eight S-band) with 250 km range provide complete
201 horizontal scan every five minutes, and provide the reflectivity factor which is directly related
202 to the precipitation rate. Sprites can then be related to the cloud system properties, to
203 determine the type of thundercloud structure that favours their production and in what
204 evolutionary phase of the convective system they are generated [Neubert *et al.*, 2008; Sao
205 Sabbas *et al.*, 2009; Soula *et al.*, 2009a].

206 **3. Results and Discussion**

207 Lightning data collected at Pic du Midi (42° 56' 11''N; 00° 08' 34''E; 2.877 km
208 altitude) in the French Pyrénées during the EuroSprites (2003-2007) campaign are analyzed
209 to understand relationship between lightning and sprites. It is noted that there are days with
210 convective clouds but neither lightning nor sprites are observed. It is known that the vast
211 majority of cloud systems having some space charge do not meet the requirements for
212 lightning. Convective clouds, with vertical motions of at least 5 to 10 ms⁻¹ and a substantial
213 depth of mixed phase precipitation (-10°C to -40°C) are required for most lightning (Lyons,
214 2006). Table 1 presents randomly selected days when lightning in Europe are recorded but
215 sprites are not observed. In figure (4), we have shown number of lightning flashes per ten
216 minutes on the August 13, 2005 and July 01, 2006. Large numbers of flashes suggest
217 thunderstorms to be deep convective system. Thus deep convective system having lightning
218 flashes may not initiate sprites. In this table there are some days on which MIL has been
219 observed and on the remaining days MIL has not been observed. Table 2 presents randomly
220 selected days when both lightning and sprites are observed. Almost on all these dates

221 evidence of MIL is also observed. *Neubert et al.* (2008) analyzed the storms of July 21, 2003;
222 July 29, 2005; September 11, 2006; and many other storms in order to separate convective
223 and stratiform precipitations. They have reported that almost all storms begin small with
224 predominantly intense convective precipitation (>50 dBZ) with a trailing stratiform
225 configuration. Sprites were observed during periods where the area of the stratiform
226 precipitation region with reflectivities from 30-45 dBZ was growing, and usually lasted until
227 the size of this region begins to decrease. For the storm systems observed during the
228 EuroSprite campaigns, sprites tended to occur when the cloud canopy reached its largest
229 extent [*Neubert et al.*, 2008 ; *Soula et al.*, 2009a]. In all these cases charge moment change
230 (ΔM_q) is large (~ 800 C km), which is the key source parameter in the initiation of sprites
231 [*Wilson*, 1925, *Huang et al.*, 1999; *Lyons* 2006]. These discussions show that there is not one
232 to one correspondence between convective cloud discharges and sprites. Only certain classes
233 of convective storms can generate cloud – to - ground discharges with the requisite large
234 ΔM_q , which could initiate sprites.

235 We have also computed the fraction of sprite days with respect to lightning days. The
236 analysis of data shows observations of sprites on 10 days and lightning on 69 days in the year
237 2003. Thus, the ratio of sprite days to lightning days is about 0.144. In the year 2005, the
238 days with sprites and lightning are 12 and 142 respectively, yielding the ratio to be about
239 0.084. The days with sprites and lightning in the year 2006 are 7 and 108 respectively. The
240 ratio is about 0.064. In 2007, the days with sprites and lightning are 8 and 132 respectively
241 and the ratio is about 0.06. The average ratio for these years comes out to be about 0.088.

242 To understand the relation between the MIL and sprites occurring above the
243 thunderstorms, temperature profiles were plotted on each of the days on which sprites are
244 observed above the thunderstorms (*Neubert and Chanrion*, 2008; *www.electricstorms.net*).
245 Figures 2 (a) to (f) exhibit typical vertical temperature structure for randomly selected

246 inversion days 22-07-2003 (near Pic), 27-07-2003 (near Puy), 11-08-2005 (near Puy), 09-09-
247 2005 (near Puy), 27-07-2006 (near Puy), and 13-10-2007 (near Pic) respectively. It is quite
248 evident that on an inversion day the temperature increases by $\sim 20\text{K}$ at about 100 km altitude.
249 At these stations the inversions occur mostly between 75-95 km.
250 Table 3 depicts the days during the campaign on which sprites are observed above the
251 stratiform region of convective thunderstorms and the respective vertical profile of
252 temperature shows the evidence of MIL on the same day. The brightest region of the sprites
253 lies in the altitude range 65-75 km, above which there is often faint red glow or wispy
254 structure that extended to about 90 km (Figure 1). Below the bright red region, tendril-like
255 filamentary structures often extend downward to as low as 40 km. Figure 3 depicts the
256 vertical temperature structure for the randomly selected typical non-inversion days (a) 25-07-
257 2003 (near Pic), (b) 26-08-2003 (near Puy), (c) 18-07-2005 (near Puy), (d) 20-07-2005 near
258 Puy, (e) 06-07-2006 (near Puy), (f) 14-10-2007 (near Pic) as recorded by SABER near Pic du
259 Midi or Puy de Dôme where simultaneously sprites are not observed on the same day at these
260 locations. Table 4 depicts the days on which sprites are not recorded during the campaign and
261 the vertical profile of temperature does not show the existence of inversion (non-inversion
262 days). In figure 5 we have presented six cases of MIL which were not associated with sprites.
263 These are explained by the fact that MILs are generated by the interaction of gravity waves
264 generated during thunderstorms with planetary waves, as well as contributions from others
265 sources [*Meriwether and Gardner, 2000*].

266 Comparing tables 1 and 4, it is noted that at least there are six days on which lightning
267 discharges have been observed but sprites and MIL have not been observed. It has already
268 been discussed that sprite-initiation requires large value of ΔM_q and hence thunderstorms on
269 those dates may not have sufficient value of ΔM_q and other required properties. Gravity
270 waves play an important role in the development of MIL [*Meriwether et al., 1998; Gardner*

271 *and Yang, 1998*]. The absence of MIL could be explained by considering the fact that either
272 gravity waves are not generated during the thunderstorm activity period or generated gravity
273 waves could not reach the mesosphere due to filtering effect of the intervening medium. Even
274 gravity waves reaching the mesosphere with small amplitudes may not be able to produce
275 observable MIL effect.

276 Convective motion associated with thunderstorms generate gravity waves which
277 propagate upwards and may get amplified [*Sentman et al., 2003; Lyons and Armstrong,*
278 *2004*]. The gravity waves become unstable at the height where the zonal wind velocity
279 becomes equal to the wave phase velocity. When this occurs, convective instability or shear
280 instability causes transfer of wave energy from gravity waves to the mean flow with
281 consequent changes in the tidal wind amplitude and phase. Usually in the mesosphere this
282 condition is satisfied and breaking of gravity waves takes place [*Sica and Thorsley, 1996;*
283 *Thomas et al., 1996*]. The turbulent heating, arising from the breaking of waves, provides a
284 feedback mechanism that then may maintain the observed MIL [*Fadnavis et al., 2007*]. The
285 plausible role of breaking gravity waves in the formation of the mid-latitude temperature
286 inversion was also pointed out by *Leblanc and Hauchecorne* [1997] and *Williams et al.*
287 [2002]. Based on the experimental and simulation results *Oberheide et al.* [2006] have
288 suggested that the interaction of gravity waves with planetary waves results in a sharp phase
289 transition of planetary waves large enough to create a MIL.

290 Convective thunderstorm generated gravity waves [*Dewan et al., 1998*] while
291 propagating upward produce perturbations in the neutral density, typically at scales of 10-50
292 km and $\Delta N/N \sim 30\%$ (where N is neutral density), as evidenced in images of OH airglow.
293 These perturbations could modulate the local threshold electric discharge field, with low
294 densities having lower thresholds [*Sentman et al., 2003; Sao Sabbas et al., 2009*]. For a
295 given charge moment change in the underlying thunderstorm the favoured initiation point for

296 sprites would be where threshold electric field is minimum [Sao Sabbes *et al.*, 2009]. Soula *et*
297 *al.* [2009b] have presented some structure sprites were linked with the electrical perturbation
298 of the elves (6 elves (4 with a sprite)) and halos (5 halos (4 with a sprite)) observed at the
299 night of 15/16 November, 2007 during the coordinated European campaign of TLE
300 observation in 2007 over the Mediterranean Sea. Neubert *et al.* [2005] had presented a
301 structured sprite cluster that was explained to have been formed in such a process. However,
302 it is not known whether the medium scale structure (~10 km) is caused by the local
303 conditions such as the turbulence field in the mesosphere or by interference patterns in the
304 radiated and reflected source electric fields [Neubert *et al.*, 2005]. The electric fields from
305 upward discharges [Krehbiel *et al.*, 2008] decrease as the inverse of the square of distance
306 whereas the threshold for electrical breakdown follows the density of air which decreases
307 exponentially. Under these circumstances there exists an altitude range, well above
308 thunderstorm, where the electric field can exceed the threshold for breakdown and initiate
309 sprites [Wilson, 1925; Huang *et al.*, 1999; Williams, 2001].

310 The sprites can change the chemical composition of the atmosphere by producing
311 NO_x and HO_x in the mesosphere and lower atmosphere [Sentman *et al.*, 2008]. Observations
312 show that N₂ is ionized during sprites [Armstrong *et al.*, 1998; Heavener, 2000]. Ionization in
313 the mesosphere is primarily in the form of positive and negative ions [Brasseur and Solomon,
314 1986] and because of their low mobility and the small electric field they would remain where
315 they are created. The ions help in the production of NO_x and HO_x. Enell *et al.* [2008] and
316 Sentman *et al.* [2008] have estimated the chemical effect of sprites in the atmosphere and
317 suggested that sprites are of little global chemical significance in producing NO_x as compared
318 to the other sources. This is supported by the measurements of NO₂ at 52 km attitude over
319 large thunderstorms which showed enhancements by ~ 10% [Arnone *et al.*, 2008]. However
320 in extraordinary cases local enhancements of NO_x may become significant, up to 5 times the

321 minimum background at 70 km. The enhancement in NO_x causes reduction in ozone in the
322 mesosphere [*Singh et al.*, 2005; *Schumann and Huntrieser*, 2007; *Sentman et al.*, 2008;
323 *Siingh et al.*, 2008]. *Fadnavis et al.* [2007] observed that the ozone concentration is halved
324 within the MIL.

325 *Sentman et al.* [2003] investigated simultaneous observations of coincident gravity
326 waves and sprites to establish an upper limit on sprite-associated thermal energy deposition in
327 the mesosphere. They estimated the resultant temperature perturbation associated with the
328 concentrically expanding gravity waves to be $\sim 7\text{K}$. The neutral temperature perturbation ΔT
329 caused by sprites $\leq 0.5\text{K}$ at the altitude ~ 85 km. The corresponding total thermal energy
330 deposited by the sprite is less than ~ 1 GJ [*Sentman et al.*, 2003]. The chemical changes by
331 sprites are fairly minor, and the heating is minuscule, and they could not be responsible in
332 producing the observed MIL. This suggests that sprites may not contribute in the production/
333 maintenance of MILs, whereas the density reductions that accompany dissipating gravity
334 waves may help in the initiation of sprites.

335 **4. Conclusions**

336 By analyzing radio soundings of the mesosphere (vertical temperature profile) and
337 optical data from the EuroSprites campaign during 2003-2007, we have shown an association
338 of sprites with the inversion in the mesospheric temperature profile, known as MIL. Gravity
339 waves generated during convective thunderstorms propagate upwards into the mesosphere;
340 they facilitate the production of MIL by depositing mechanical energy and momentum into
341 this region from below. Gravity waves also modulate the neutral air density in the
342 mesosphere. The intense electric fields caused by the charge imbalance in the stratiform
343 regions of convective thunderstorm after a CG flash penetrates into the mesosphere and
344 initiate the production of sprites. Modulation of the neutral air density and heating by gravity

345 waves aid the initiation process of sprites and hence explain the association of sprites with
346 MILs.

347 Further, observations of both MIL and lightning without sprites have been explained
348 by considering the generation of gravity waves during deep convective activity and its
349 propagation to mesosphere where they may help in the production of MIL and modulation of
350 neutral density. However, convective systems with weak ΔM_q will not be able to initiate
351 sprite and thus one can explain the observation of MIL and lightning without sprite.

352 The observation of lightning without MIL and sprite is easily explained by
353 considering the fact that gravity waves are not able to reach the mesosphere. This situation
354 may arise either due to absorption/filtering effect of gravity wave by the ambient medium or
355 by the non-generation of gravity wave during thunderstorm activity. Further, case-by-case
356 study is required.

357 **Acknowledgements**

358 The authors thank to Dr Torsten Neubert and Dr O. Chanrion for providing sprite and
359 lightning data. One of the authors (Devendraa Siingh) wishes to thank Dr Torsten Neubert for
360 general discussion on Sprites and MIL during his visit to the Danish National Space Center
361 (DNSC), Copenhagen, Denmark. DS expresses his gratitude to Dr Jens Olaf P Pedersen for
362 extending an invitation to visit DNSC. SF and DS acknowledge the Ministry of Earth
363 Sciences, Government of India for financial support and also thanks to Dr. B. N. Goswamy,
364 Director IITM, for his encouragement.

365 The authors thank anonymous reviewers (I & III reviewer) for their critical comments
366 and valuable suggestions, which helped in improving the scientific value of this research
367 paper. They also express their gratitude to Dr. E. R. Williams (II reviewer, MIT, USA) for a
368 comprehensive and very thorough review, which resulted in significant improvements in the
369 manuscript.

370 **References**

- 371 Armstrong, R.A., J.A. Shorter, M.J. Taylor, D.M. Suszcynsky, W.A. Lyons, and L. S. Jeong
372 (1998), Photometric measurements in the SPRITES'95 & 96 campaigns of nitrogen
373 second positive (399.8nm) and first negative (427.8nm) emissions, *J. Atmos. Solar*
374 *Terr. Phys.*, 60, 787-799.
- 375 Arnone, E., P. Berg, F. Boberg, J. Bor, O. Chanrion, C.-F., Enell, M. Ignaccola, A. Mika, A.
376 Odzimek, O. Van der Velde, T. Farges, S. Laursen, T. Neubert, and G. Satori (2008),
377 The Eurosprites 2005 campaign, in Proceeding of the 33rd annual European meeting
378 on atmospheric studies by optical methods (33AM), edited by J. Arvelius, No 292 in
379 IRF Scientific Reports, Swedish Inst. of Space Physics, Kiruna.
- 380 Barrington-Leigh, C.P., U. S. Inan, M. Stanley, and S.A. Cummer (1999), Sprites triggered
381 by negative lightning discharges, *Geophys. Res. Lett.* 26 (24), 3605–3608.
- 382 Bell, T.F., V.P. Pasko, and U.S. Inan (1995), Runaway electrons as a source of red sprites in
383 the mesosphere, *Geophys. Res. Lett.*, 22, 2127-2130.
- 384 Boccippio, D.J., E.R. Williams, S.J. Heckman, W.A. Lyons, I.T. Baker, and R. Boldi,
385 (1995), Sprites, ELF transients, and positive ground strokes, *Science* 269,1088-1091.
- 386 Brasseur, G., and S. Solomon (1986), *Aeronomy of the Middle atmosphere*, Atmospheric
387 Science Library, D. Reidel Publishing Company.
- 388 Chanrion, O., N. B. Crosby, E. Arnone, F. Boberg, O. Van der Velde, A. Odzimek, A. Mika,
389 C.-F. Enell, P. Berg, M. Ignaccolo, R. J. Steiner, S. Laursen, and T. Neubert (2007),
390 The Eurosprite 2005 observational campaign: An example of training and outreach
391 opportunities for CAL young scientist, *Advances in Geosciences* , 13, 3-9
- 392 Christensen, A. B., R. L. Walterschied, M. N. Ross, C.-I. Meng, L. J. Paxton, D.
393 Anderson, G. Crowley, S. Avery, R. Meier, and D. Strickland (2004), Global

394 Ultraviolet Imager for the NASA TIMED Mission, *SPIE Optical Spectroscopic*
395 *Techniques and Instrumentation. Atmospheric and Space Research*, 2266, 451-466.

396 Chu, X., C. S. Gardner, and S. J. Franke (2005), Nocturnal thermal structure of the
397 mesosphere and lower thermosphere region at Maui, Hawaii (20.7° N), and Starfire
398 optical range, New Mexico (35°), *J. Geophys. Res.*, 110, D09S03, doi:
399 1029/2004JD004891.

400 Cummins, K.L., M. J. Murphy, E. A. Bardo, W. L. Hisco, R. B. Pyle, and A. E. Pifer (1998)
401 A combined TOA/MDF technology upgrade of the US National Lightning Detection
402 Network, *J. Geophys. Res.*, 103, 9035-9044.

403 Dewan, E. M., R. H. Picard, R. R. O'Neil, H. A. Gardiner, J. Gibson, J.D. Mill, E. Richards,
404 M. Kendra, and W.O. Gallery (1998), MSX satellite observations of thunderstorm-
405 generated gravity waves in mid-wave infrared images of the upper stratosphere,
406 *Geophys. Res. Lett.*, 25, 939-942.

407 Drue, C., T. Hauf, U. Finke, S. Keyn, and O. Hreyer (2007), Comparison of a SAFIR
408 lightning detection network in northern Germany to the operational BLIDS network,
409 *J. Geophys. Res.*, 112D18114, doi:10.1029/2006JD007680.

410 Enell, C.-F., E. Arnone, T. Adachi, O. Chanrion, P. T. Verronen, A. Seppala, T. Neubert, T.
411 Ulich, E. Turunen, Y. Takahashi and R.-R. Hsu (2008), Parameterisation of chemical
412 effect of sprites in the middle atmosphere, *Ann. Geophys.*, 26, 13-27, 2008.

413 Fadnavis, S and G. Beig (2004), Mesospheric temperature inversions over the Indian tropical
414 region, *Ann. Geophys.*, 22, 3375-3383.

415 Fadnavis, S., Devendraa Siingh, G. Beig, and R. P. Singh (2007), Seasonal variation of the
416 mesospheric inversion layer, thunderstorm and ozone over India, *J. Geophys. Res.*,
417 112, D15305, doi:10.1029/2006JD008379.

418 Fovell, R. G., and Y. Ogura (1989), Effect of the vertical wind shear on numerically
419 simulated multicell storm structure, *J. Atmos. Sci.*, 46, 3144–3176.

420 Gardner, C. S., and W. Yang (1998), Measurement of the dynamical cooling rate associated
421 with the vertical transport of heat by dissipating gravity waves in the mesopause
422 region at the surface optical range, New Mexico, *J. Geophys. Res.*, 103, 16 909-
423 16,926.

424 Gordillio-Vazquez, F. J (2008), Air plasma kinetics under the influence of sprites, *J Phys D*
425 *Appl Phys* 41(234016):33. doi:10.1088/0022-3727/41/23/234016.

426 Haldoupis, C., R. J. Steiner, A. Mika, S. Shalimov, R. A. Marshall, U. S. Inan, T. Bosinger,
427 and T. Neubert, (2006), “Early/slow” events: a new category of VLF perturbations
428 observed in relation with Sprites, *J. Geophys. Res.*, 111, A11321 1-9,
429 doi:10.1029/2006JA011960, 2006.

430 Hauchecorne, A., and A. Maillard (1990), A 2-D dynamical model of mesospheric
431 temperature inversions in winter, *Geophys. Res. Lett.*, 17, 2197-2200.

432 Hauchecorne, A., M. L. Chanin, and R. Wilson (1987), Mesospheric temperature inversion
433 and gravity wave breaking, *Geophys. Res. Lett.*, 14, 933–936.

434 Heavner, M. J. (2000), Optical spectroscopic observations of sprites, blue jets and elves:
435 Inferred microphysical processes and their microphysical implications, Ph.D. thesis,
436 University of Alaska, Fairbanks, Alaska.

437 Huang, E., E. R. Williams, R. Boldi, S. Heckman, W. Lyons, M. Taylor, T. Nelson, and C.
438 Wong (1999), Criteria for sprites and elves based on Schumann resonance
439 observations, *J. Geophys. Res.*, 104, 16943-19969.

440 Krehbiel, P. R., J. A. Riousset, V. P. Pasko, R. J. Thomas, W. Rison, M. A. Stanley, and H.
441 E. Edens (2008), Upward electric discharges from thunderstorms. *Nature Geoscience*,
442 1, 233-237.

443 Kumar, V. S., Y. B. Kumar, K. Raghunath, P. B. Rao, M. Krishnaiah, K. Mizutani, A. Aoki,
444 M. Yasui, and T. Itabe (2001), Lidar measurements of mesospheric temperature
445 inversion at low latitude, *Ann. Geophys.*, 19, 1039-1044.

446 Leblanc, T., and A. Hauchecorne (1997), Recent observations of mesospheric temperature
447 inversions, *J. Geophys. Res.*, 102, 19471-19482.

448 Leblanc, T., A. Hauchecorne, M. L. Chanin, F. W. Taylor, C. D. Rodgers, and N. Livesey
449 (1995), Mesospheric inversions as seen by ISAMS (UARS), *Geophys. Res. Lett.*, 22,
450 1485-1488.

451 Lehtinen, N., T. Bell, V. Pasko, and U. Inan, (1997), A two-dimensional model of runaway
452 electron beams driven by quasi-electrostatic thundercloud fields, *Geophys. Res. Lett.*,
453 24, 2639-2642.

454 Liu, H.L., and M.E. Hagan (1998), Local heating/cooling of the mesosphere due to gravity
455 wave and tidal coupling, *Geophys. Res. Lett.*, 25, 2941-2944.

456 Liu, H.L., M.E. Hagan, and R.G. Roble (2000), Local mean state changes due to gravity
457 wave breaking due to modulated by diurnal tides, *J. Geophys. Res.*, 105, 12381-
458 12396.

459 Lyons, W.A. (2006), The meteorology of transient luminous events-an introduction and
460 overview, in *Sprites, Elves and intense lightning discharge*, Fullekrug, M. et al. (eds)
461 Vol. 225 of NATO Science series to Mathematics, Physics and Chemistry, pp 19-56,
462 Springer, Verlag, ISBN, 1-4020-4628-6.

463 Lyons, W.A., and R.A. Armstrong, (2004) A review of electrical and turbulence effects of
464 convective storms on the overlying stratosphere and mesosphere, AMS Symposium
465 on Space Weather, AMS Annual Meeting, Seattle, WA, 10-15, January, 2004 6 pp,
466 published on conference CD.

467 Lyons, W.A., R.A. Armstrong, E.A. Bering III, and E.R. Williams, (2000), The hundred year
468 hunt for red sprite, *EOS, Trans. AGU*, 81(33), 373-377.

469 Mazur, V., X. M. Shao, and P.R. Krehbiel, (1998), Spider lightning in intra-cloud and
470 positive cloud-to-ground flashes, *J. Geophys. Res.*, 103(D16), 19811-19822,
471 doi:10.1029/98JD02003

472 Mertens, C.J., F. J. Schmidlin, and R.A. Goldberg (2004), SABER observations of
473 mesospheric temperatures and comparisons with rocket falling sphere measurements
474 taken during the 2002 summer MaCWAVE campaign, *Geophys. Res. Lett.*, 31,
475 L03105, doi: 10.1029/2003GL018605.

476 Meriwether, J. W., and C. S. Gardner (2000), A review of the mesospheric inversion layer
477 phenomenon, *J. Geophys. Res.*, 105, 12405- 12416.

478 Meriwether, J. W., and A.J. Gerrard (2004) Mesospheric inversion layers and stratospheric
479 temperature enhancements, *Rev. Geophys.*, 42(3) doi:10.1029/2003RG0001333.

480 Meriwether, J. W., X. Gao, V. B. Wickwar, T. Wilkerson, K. Beissner, S. Collins, and M.
481 Hagan (1998), Observed coupling of the mesospheric inversion layer to the thermal
482 tidal structure, *Geophys. Res. Lett.*, 25, 1479-1482.

483 Mika, A., C. Haldoupis, R. A. Marshall, T. Neubert, and U.S. Inan (2005), Subionospheric
484 VLF signatures and their association with sprites observed during EuroSprite-2003,
485 *J. Atmos. Solar Terr. Phys.*, **67**, 1580-1597.

486 Mlynczak, M. G., and S. Solomon (1993), A detailed evaluation of the heating efficiency in
487 the middle atmosphere, *J. Geophys. Res.*, 98, 10,517– 10,541.

488 Neubert, T. (2003), On sprites and their exotic kin, *Science* 300, 747-748.

489 Neubert, T. and O. Chanrion (2008), Personal communication with Devendraa Siingh during
490 visit to the Danish National Space Center (DNSC), Copenhagen, Denmark.

491 Neubert, T., et al., (2005), Co-ordinated observations of transient luminous events during the
492 EuroSprite2003 campaign, *J. Atmos. Solar Terr. Phys.* 67, 807–820.

493 Neubert, T. et al, (2008), Recent results from studies of electric discharges in the
494 mesosphere, *Surv. Geophys.* 29, 71-137.

495 Oberheide, J., H. L. Liu, O.A. Gusev, and D. Offermann (2006), Mesospheric Surf zone and
496 temperature inversion layers in early November 1994, *J. Atmos. Solar Terr. Phys.*, 68,
497 1752-1763.

498 Pasko, V. P., U.S. Inan, Y. Taranenko, and T. F. Bell (1995), Heating, ionization and upward
499 discharges in the mesosphere due to intense quasi-electrostatic thundercloud fields,
500 *Geophys. Res. Lett.*, 22, 365–368.

501 Picard, R. H., U. S. Inan, V.P. Pasko, J. R. Winick, and P. P. Wintersteiner (1997), Infrared
502 glow above thunderstorms? *Geophys. Res. Lett.*, 24, 2635-2638.

503 Picard, R. H., R. R. O’Neil, H. A. Gardiner, J. Gibson, J. R. Winick, W. O. Gallery, Jr. A. T.
504 Stair, P. P. Wintersteiner, E.R. Hegblom, and E. Richards (1998), Remote sensing of
505 discrete stratospheric gravity-wave structure at 4.3 μm from MSX satellite, *Geophys.*
506 *Res. Lett.*, 25, 2809 -2912.

507 Rodger, C.J., A. Seppala and M.A. Clilverg (2008), Significance of transient luminous
508 events neutral chemistry: experimental measurements, *Geophys. Res. Lett.*, 35,
509 L07803 doi: 10.1029/2008GL033221.

510 Roussel-Dupre, R.A., and A.V. Gurevich (1996), On runaway breakdown and upward
511 propagating discharges, *J. Geophys. Res.*, 101, 2297-2311.

512 Sao Sabbas F. T., et al. (2009), Characteristics of sprite and gravity wave convective sources
513 present in satellite IR images during the SpreadFEx 2005 in Brazil, *Ann. Geophys.*,
514 27, 1279-1293.

515 Schumann, U., and H. Huntrieser (2007), The global lightning induced nitrogen oxides
516 source, *Atmos. Chem. Phys.*, 7, 3823-3907.

517 Schmidlin, F. J. (1976), Temperature inversion near 75 km, *Geophys. Res. Lett.*, 3, 173-176.

518 Sentman, D. D., E. M. Wescott, R. H. Picard, J. R. Winick, H. C. Stenbaek-Nielsen, E. M.
519 Dewan, D. R. Moudry, F. T. São Sabbas, M. J. Heavner, and J. Morrill (2003),
520 Simultaneous observations of mesospheric gravity waves and sprites generated by a
521 midwestern thunderstorm, *J. Atmos. Solar Terr. Phys.*, 65, 537-550.

522 Sentman, D. D., H. C. Stenbaek-Nielsen, M. G. McHarg, and J. Morrill (2008), Plasma
523 chemistry of sprite streamers, *J. Geophys. Res.*, 113, D11112,
524 doi:10.1029/2007SD008941.

525 Sica, R. J., and M. D. Thorsley (1996), Measurements of super adiabatic lapse rates in the
526 middle atmosphere, *Geophys. Res. Lett.*, 23, 2797-2800.

527 Siingh, Devendraa et al. (2005), Review of electromagnetic coupling between the earth's
528 atmosphere and the space environment, *J. Atmos. Solar Terr. Phys.*, 67, 637-658.

529 Siingh, Devendraa, V. Gopalakrishnan, R.P. Singh, A.K. Kamra, S. Singh, V. Pant, R.
530 Singh, and A.K. Singh (2007), The atmospheric global electric circuit: An overview,
531 *Atmos. Res.*, 84, 91-110.

532 Siingh, Devendraa, A.K. Singh, R.P. Patel, R. Singh, R.P. Singh, B. Veenadhari, M.
533 Mukherjee, (2008), Thunderstorm, lightning, sprites and magnetospheric whistler
534 mode radio waves, *Surv. Geophys.*, 29, 499-551, doi: 10.1007/s10712-008-9053-z.

535 Singh, D.K., R.P. Singh, and A.K. Kamra (2004), The electrical environment of the Earth's
536 atmosphere: a review, *Space Sci. Rev.*, 113, 375-408.

537 Singh, R.P., R. P. Patel, R. Singh, and R.N. Singh (2005), Lightning produced nitrogen
538 oxides in the lower atmosphere: An overview, *Indian J. Radio Space Phys.*, 34, 248-
539 254.

540 Soula, S., Oscar van der Velde, J. Montanyà, T. Neubert, O. Chanrion, and M. Ganot
541 (2009a), Analysis of thunderstorm and lightning activity associated with sprites
542 observed during the EuroSprite campaigns: Two case studies, *Atmos. Res.*, 91, 514-
543 528

544 Soula, S., Oscar van der Velde, J. Palmieri, O. Chanrion, J. Montanyà and F. Lefeuvre
545 (2009b), Characteristics and conditions of production of TLEs observed over a
546 Maritime storm, in *AGU Chapman conference on the effects of thunderstorms and*
547 *lightning in the upper atmosphere*, Penn State University, State College, PA, USA,
548 10-14, May, 2009

549 States, R. J., and C. S. Gardner (1998), Influence of the diurnal tide and thermospheric heat
550 sources on the formation of mesospheric temperature inversion layers, *Geophys. Res.*
551 *Lett.*, 25, 1483.

552 Swenson, B. R., and A. Z. Liu, (1998), A model for calculating acoustic gravity wave energy
553 and momentum flux in the mesosphere from OH airglow, *Geophys. Res. Lett.*, 25,
554 477-480.

555 Taranenkov, Y., and R. Roussel-Dupre (1996) High altitude discharges and gamma-ray
556 flashes: a manifestation of runaway air breakdown, *Geophys. Res. Lett.*, 23, 571-574.

557 Taylor, M. J., and M. J. Hill, (1991), Near infrared imaging of hydroxyl wave structure over
558 an ocean site at low latitude, *Geophys. Res. Lett.*, 18, 1333-1336.

559 Thomas, L., A. K. P. Marsh, D.P. Wareing, I. Astin, and H. Changra, (1996), VHF echoes
560 from the mid latitudes mesosphere and the thermal structure observed by lidar, *J.*
561 *Geophys. Res.*, 101, 12867-12877.

562 Turnbull, D. N., and R. P. Towe (1991), Temporal variation in the hydroxyl nightglow
563 observed during ALOHA-90, *Geophys. Res. Lett.*, 18, 1345-1348.

564 Williams, B.P., M.A. White, D.A. Krueger, and C.Y. She (2002), Observation of a large
565 amplitude wave and inversion layer leading to convective instability in the mesopause
566 region over Fort Collins, CO (41N, 105W), *Geophys. Res. Lett.*, 29(17), 1850,
567 doi:10.1029/2001GL014514, 2002.

568 Williams, E.R., (1998), The positive charge reservoir for sprite-producing lightning, *J.*
569 *Atmos. Solar Terr. Phys.*, 60, 689-692.

570 Williams, E.R. (2001), Sprites, elves and glow discharge tubes, *Phys. Today (September*
571 *issue)*, 1-7.

572 Williams, E. R., M., Valente, E. Gerken and R. Golka, 2006: Calibrated radiance
573 measurements with an air-filled glow discharge tube: application to sprites in the
574 mesosphere. In: "Sprites, Elves and Intense Lightning Discharges", M. Fullekrug et al.
575 (eds.), 237-247, Springer (Printed in the Netherlands).

576 Williams, E. R, E. Downes, R. Boldi, W. Lyons, and S. Heckman, (2007), Polarity
577 asymmetry of sprite-producing lightning: a paradox? *Radio Sci.* 42, RS2S17.
578 doi:10.1029/2006RS003488.

579 Wilson, C.T.R. (1925), The effect of a thundercloud and some of its effects, *Proc, Phys. Soc.*
580 *London*, 37, 32D-37D.

581 Wu, Q. and T.L. Killeen (1996), Seasonal dependence of mesospheric gravity waves (<100
582 km) at Peach Mountain Observatory, Michigan, *Geophys. Res. Lett.*, 23, 2211–2214.
583
584
585
586
587
588

589 **Legends**

590 Figure 1: Diagram showing the standard vertical thermal structure of the atmosphere, a
591 temperature profile obtained from the SABER instrument aboard the TIMED
592 satellite (blue profile) showing a MIL, where a MIL occurs above the
593 thunderstorm (modified figure after Lyons et al., 2000; Neubert, 2003).

594 Figure 2: Vertical temperature structure for the randomly selected typical inversion days
595 (a) 22-07-2003 (near Pic du Midi), (b) 27-07-2003 (Puy de Dôme), (c) 11-08-
596 2005 (near Puy de Dôme), (d) 09-09-2005 (near Puy de Dôme), (e) 27-07-
597 2006 (near Puy de Dôme), (f) 13-10-2007 (near Pic du Midi) as recorded by
598 SABER, where simultaneously sprites are observed above stratiform region of
599 convective thunderstorms on the same day.

600 Figure 3: Vertical temperature structure for the randomly selected typical non-inversion
601 days (a) 25-07-2003 (near Pic du Midi), (b) 26-08-2003 (near Puy de Dôme),
602 (c) 18-07-2005 (near Puy de Dôme), (d) 20-07-2005 (near Puy de Dôme), (e)
603 06-07-2006 (near Puy de Dôme), (f) 14-10-2007 (near Pic) as recorded by
604 SABER, where simultaneously sprites are not observed on the same day.

605 Figure 4: The variation of lightning flashes per ten minutes with time recorded at the Pic
606 du Midi ($42^{\circ} 56' 11''$ N; $00^{\circ} 08' 34''$ E; 2.877 km altitude) in the French
607 Pyrénées on August 13, 2005 and July 01, 2006.

608 Figure 5: Vertical temperature structure for the randomly selected typical inversion
609 days, which were not associated with sprites; (a) 31-07-2003, (b) 09-08-2003,
610 (c) 08-07-2005, (d) 25-10-2005, (e) 23-07-2006 and (f) 23-08-2006

Table 1: Days (year-month-day) on which lightning are observed but no evidence of sprites at Pic du Midi ($42^{\circ} 56' 11''$ N; $00^{\circ} 08' 34''$ E; 2.877 km altitude) in the French Pyrénées

Day of observation	Occurrence of lightning	Range of times, lightning were observed (but no sprite), UT hr: min	Occurrence of Sprite
2003-07-25	Yes	11:44 – 18:03	No
2003-07-26	Yes	01:56 – 23:59	No
2003-07-29	Yes	00:00 – 23:15	No
2003-08-01	Yes	01:56 – 23:59	No
2003-08-16	Yes	00:00 – 23:59	No
2003-08-26	Yes	00:00 -18:07	No
2005-07-12	Yes	00:40 – 23:59	No
2005-07-15	Yes	06:29 – 23:59	No
2005-08-13	Yes	11:22 – 22:38	No
2005-08-17	Yes	00:45 – 23:59	No
2005-09-06	Yes	00:00 – 23:59	No
2005-09-19	Yes	00:00 – 23:59	No
2005-10-30	Yes	06:19 – 23:59	No
2006-06-26	Yes	00:00 – 23:59	No
2006-07-01	Yes	00:00 – 23:59	No
2006-07-10	Yes	14:41- 22:24	No
2006-08-06	Yes	00:00 – 21:12	No
2006-08-15	Yes	00:00 – 23:59	No
2007-07-30	Yes	00:00 – 23:59	No
2007-08-05	Yes	00:00 – 23:59	No
2007-08-10	Yes	00:00 – 23:59	No
2007-08-11	Yes	00:00 – 23:59	No
2007-08-30	Yes	00:00 – 23:59	No
2007-09-01	Yes	00:00 – 23:24	No
2007-09-15	Yes	00:00 – 22:08	No
2007-09-30	Yes	00:00 – 23:59	No

Table 2: Days (year-month-day) on which lightning and sprites are observed at Pic du Midi

(42° 56' 11''N; 00° 08' 34''E; 2.877 km altitude) in the French Pyrénées

Day of observation	Occurrence of lightning	Range of times, lightning were observed, UT hr:min	Occurrence of Sprite	Range of times, sprites were observed, UT hr:min
2003-07-21	Yes	00:00 – 23:59	Yes	02:05 - 03:15
2003-07-22	Yes	00:00 – 23:59	Yes	21:50 - 21:57
2003-07-23	Yes	00:00 – 23:59	Yes	21:11 – 23:21
2003-07-24	Yes	00:00 – 23:59	Yes	00:23 - 00:33
2005-07-29	Yes	00:00 – 23:59	Yes	01:28 – 02:04
2005-08-11	Yes	00:00 – 23:59	Yes	22:44 – 23:12
2005-09-09	Yes	00:00 – 23:59	Yes	01:81 – 21:18
2005-09-26	Yes	00:00 – 23:59	Yes	01:06 – 03:38
2006-07-04	Yes	00:00 – 23:59	Yes	20:46 – 22:51
2006-07-05	Yes	00:00 – 23:59	Yes	00:04 – 03:05
2006-07-22	Yes	00:00 – 23:59	Yes	01:46 – 02:01
2006-07-27	Yes	00:00 – 23:59	Yes	01:13 – 02:36
2006-08-17	Yes	00:00 – 23:59	Yes	22:29 – 23:57
2006-08-18	Yes	00:00 – 23:59	Yes	00:14
2007-08-29	Yes	00:00 – 23:59	Yes	20:11 – 20:37
2007-09-17	Yes	00:00 – 23:59	Yes	21:25 – 22:01
2007-10-13	Yes	00:00 – 23:59	Yes	00:05 – 03:54
2007-10-18	yes	00:00 – 23:59	yes	03:00

Table 3: Inversion days (year-month-day) observed in the SABER temperature profile and at least one sprite reported in the vicinity ($3^0 \times 3^0$ grid) on the same day (* indicate the plots of the given date)

Date	Existence of sprite		Evidence of MIL in SABER temperature profile at the location		Range of times, sprites were observed, UT	Time of SABER temperature profile (UT)
	Lat. degrees N	Long. degrees E	Lat. degrees N	Long. degrees E	hr:min	hr:min:sec
2003-07-21	46.8	4.1	46.2	5.2	02:05 - 03:15	03:33:26
2003-07-22 *	45.0	5.6	42.3	3.0	21:50 - 21:57	07:16:23
2003-07-23	43.9	5.9	41.6	6.4	21:11 - 23:21	02:28:23
2003-07-24	44.6	6.8	46.1	7.6	00:23 - 00:33	02:47:56
2003-07-27 *	46.5	9.7	44.3	6.2	20:46 - 21:13	02:01:25
2003-08-20	45.1	6.8	47.3	8.5	20:19	01:00:19
2003-08-25	42.7	10.8	40.1	10.2	19:56 - 21:37	00:52:52
2003-08-28	45.5	5.6	43.0	9.0	20:18 - 23:34	19:17:24
2003-08-29	46.0	6.0	48.0	4.0	00:04 - 02:35	22:59:46
2005-07-19	45.3	9.9	47.9	10.4	00:46	03:37:18
2005-07-29	45.2	2.6	45.0	5.5	01:28 - 02:04	01:29:03
2005-08-11 *	43.5	6.7	42.0	2.0	22:44 - 23:12	03:40:13
2005-08-16	41.9	0.8	48.4	1.7	23:06	22:38:43
2005-09-09 *	43.84	5.46	43.7	6.1	01:81 - 21:18	21:19:32
2005-10-23	40.6	3.7	41.1	8.8	18:59	17:19:03
2005-11-11	40.5	3.3	40.6	3.6	00:56 - 02:56	23:40:29
2006-07-04	44.3	-0.808	41.3	5.4	20:46 - 22:51	02:03:21
2006-07-27 *	45.9	1.0	11.1	0.9	01:13 - 02:36	11:57:36
2006-08-18	44.7	5.9	41.9	5.8	00:14	20:52:26
2007-08-29	46.2	6.9	46.3	9.8	20:11 - 20:37	22:40:25
2007-09-17	44.6	5.4	41.8	9.5	21:25 - 22:01	14:38:13
2007-10-13 *	37.7	5.8	38.7	3.7	00:05 - 03:54	05:22:02
2007-10-18	39.44	1.1	36.2	2.7	03:00	18:32:26

Table 4: Non inversion days (year-month-day) observed in the SABER temperature profile and no sprite reported in the vicinity ($3^0 \times 3^0$ grid) on the same day (* indicate the plots of the given date)

Day of observation	No evidence of sprite at the location		No evidence of MIL in SABER temperature profile at the location		Range of times, lightning were observed (but no sprite), UT	Time of SABER temperature profile (UT)
	Lat. degrees N	Long. degrees E	Lat. degrees N	Long. degrees E	hr:min	hr:min:sec
2003-07-25 *	44.0	5.8	48.7	8.0	11:44 – 18:03	03:06:56
2003-07-29	47.1	9.5	48.4	2.2	00:00 – 23:15	02:38:25
2003-07-30	47.1	9.5	45.0	10.0	00:29 – 23:59	01:16:20
2003-08-21	45.1	6.8	45.9	4.7	00:00 – 23:59	01:18:22
2003-08-26 *	42.0	11.0	44.0	13.8	00:00 – 18:07	23:48:14
2003-08-27	46.9	10.4	46.0	9.8	00:24 – 23:59	18:58:49
2003-08-30	46.9	10.4	44.7	7.8	00:00 – 23:59	23:19:29
2003-08-31	46.9	10.4	49.6	10.6	00:26 – 23:59	21:56:11
2005-07-18 *	45.3	9.9	45.2	10.6	00:00 – 23:59	03:19:09
2005-07-20 *	45.3	9.9	48.9	6.7	14:02 – 17:49	03:54:35
2005-07-28	45.3	9.9	43.0	8.6	00:00 – 23:59	01:11:30
2005-07-30	46.2	3.6	47.6	4.7	00:00 – 23:59	01:47:05
2005-08-09	43.9	6.8	45.0	10.8	00:00 – 23:59	03:05:45
2005-08-10	43.9	6.8	42.8	7.9	00:00 – 23:59	03:23:23
2005-08-12	43.9	6.8	47.8	4.0	00:00 - 18:59	23:09:29
2005-08-13	43.8	6.8	42.8	10.9	11:22 - 23:59	02:35:40
2005-08-14	43.9	6.8	42.4	1.5	00:00 – 23:59	22:02:08
2005-08-15	43.9	6.8	48.3	8.2	00:00 – 23:59	01:28:17
2005-08-17	43.8	7.0	42.6	7.3	00:45 - 23:59	02:04:34
2005-09-05	43.0	6.0	46.5	3.9	00:00 – 23:59	21:49:12
2005-09-06	41.0	0.8	37.2	2.8	00:00 – 23:59	16:59:05
2005-09-08	43.0	5.4	46.4	7.4	00:00 – 23:59	21:01:35
2005-09-15	43.9	6.8	46.2	2.3	02:40 - 23:59	22:20:45
2005-09-25	43.0	3.2	41.5	2.0	04:01 – 23:59	09:11:04
2005-09-26	40.12	3.8	40.8	4.8	00:00 – 23:59	22:52:00
2006-07-06 *	45.1	2.6	43.0	4.8	00:00 – 23:59	00:59:24
2006-08-19	45.5	5.1	45.2	4.7	00:00 – 23:59	21:10:25
2007-10-12	36.1	9.9	38.8	10.7	00:00 – 23:59	05:05:53
2007-10-14 *	38.0	2.6	38.0	6.2	00:00 – 22:11	19:04:01

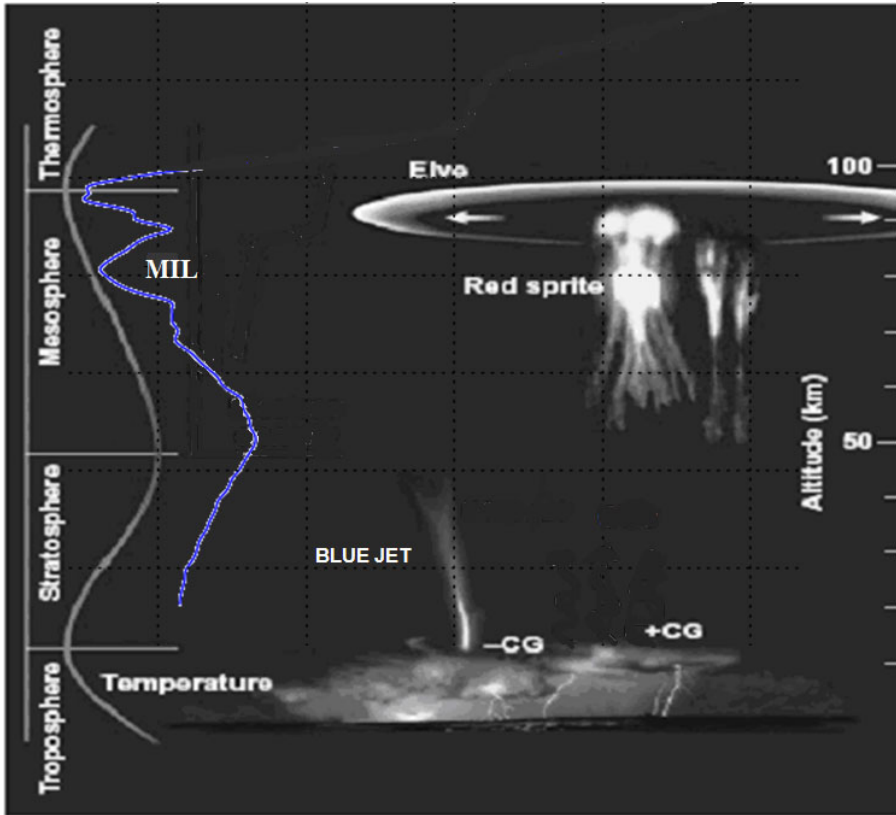


Figure.1

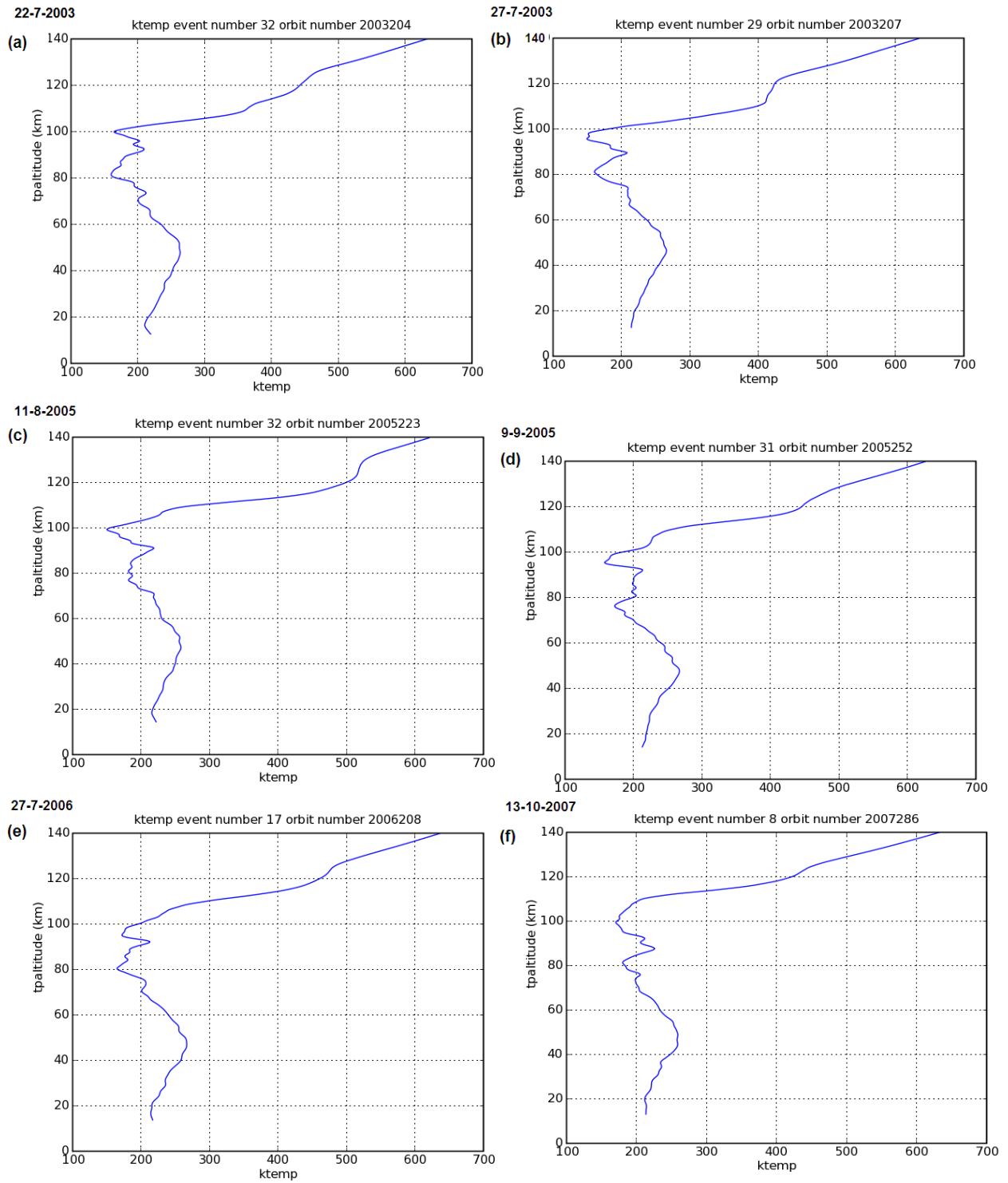


Figure 2

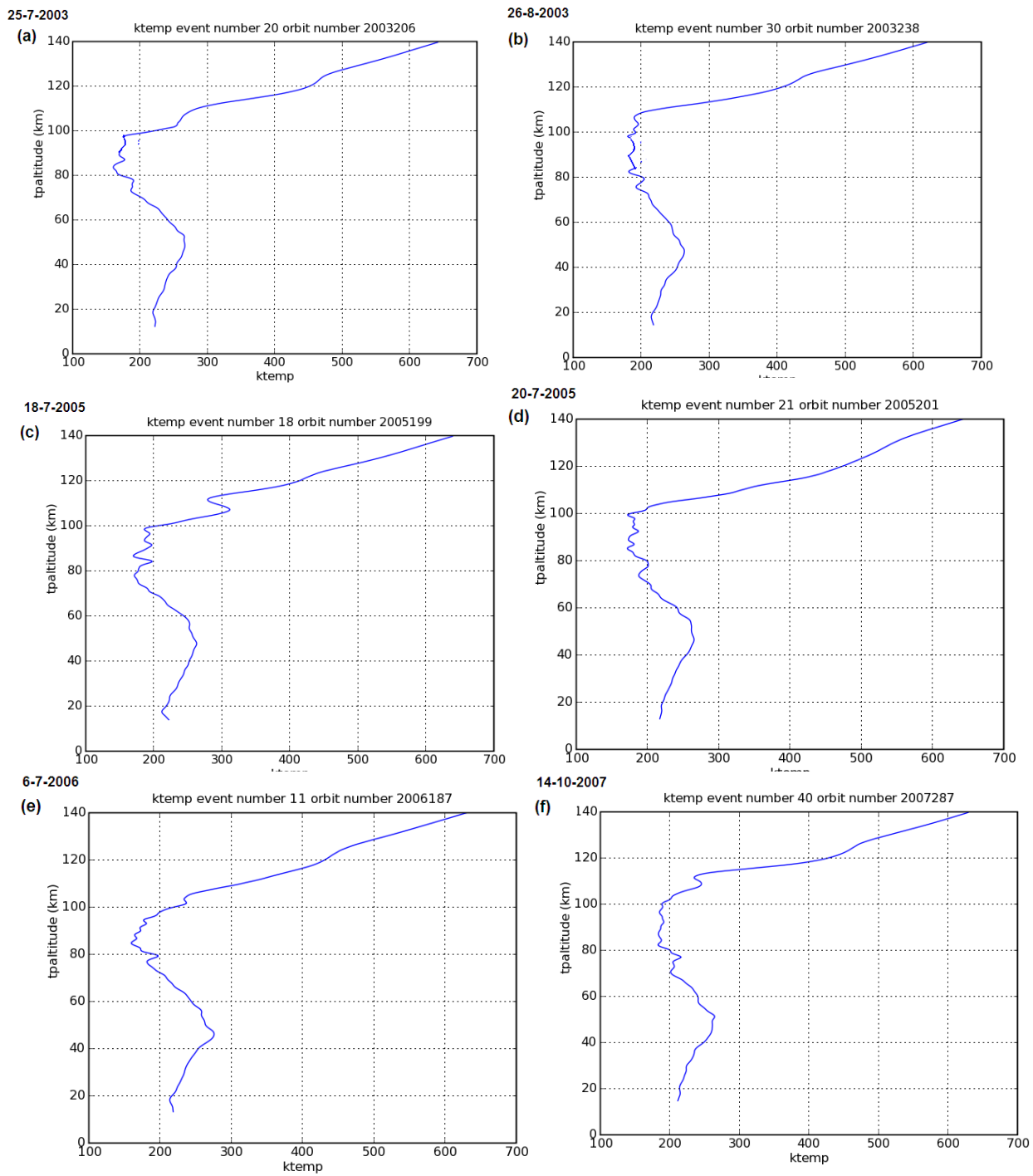


Figure 3

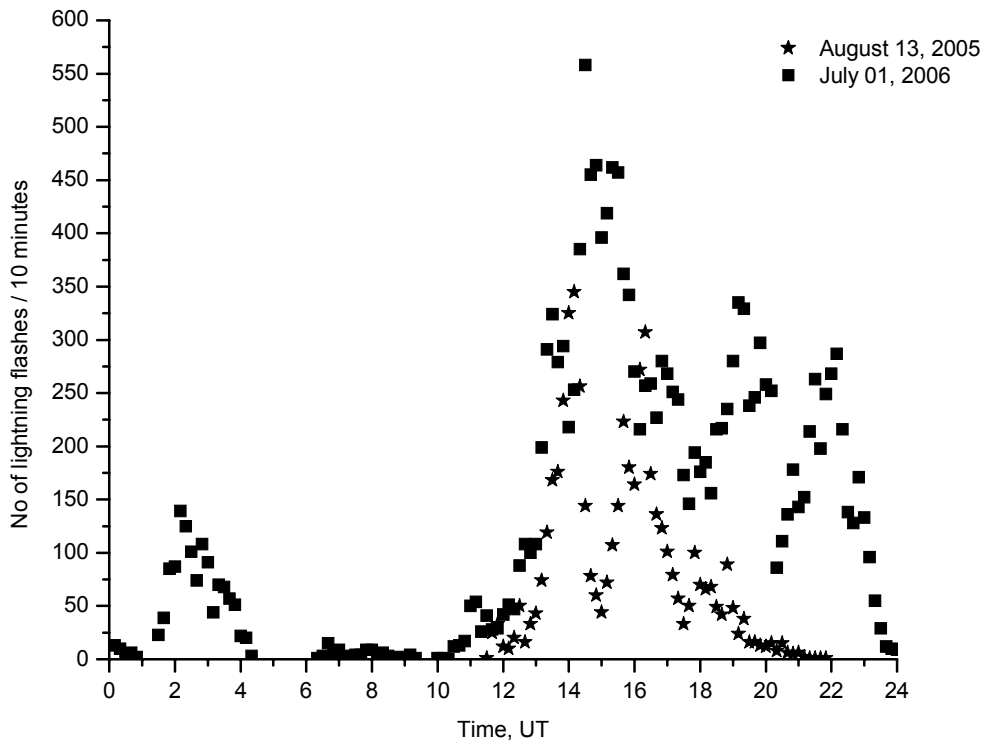
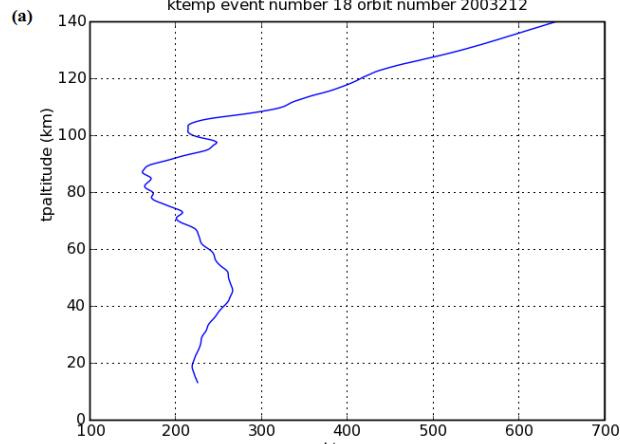
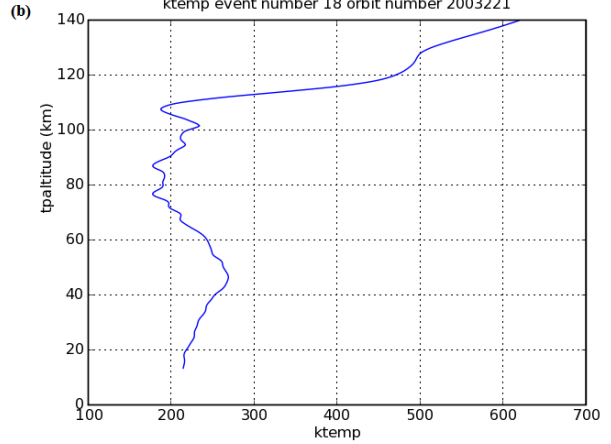


Figure 4

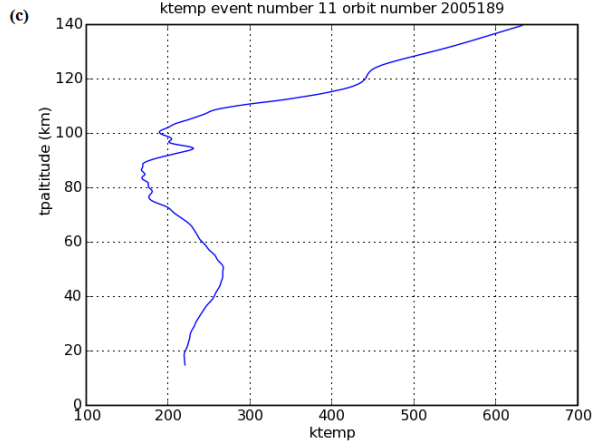
31-7-2003



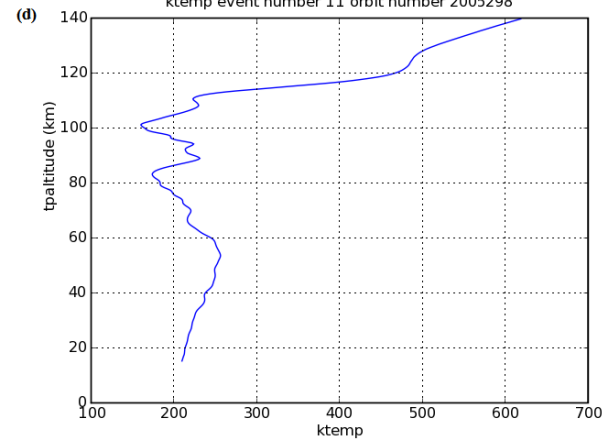
9-8-2003



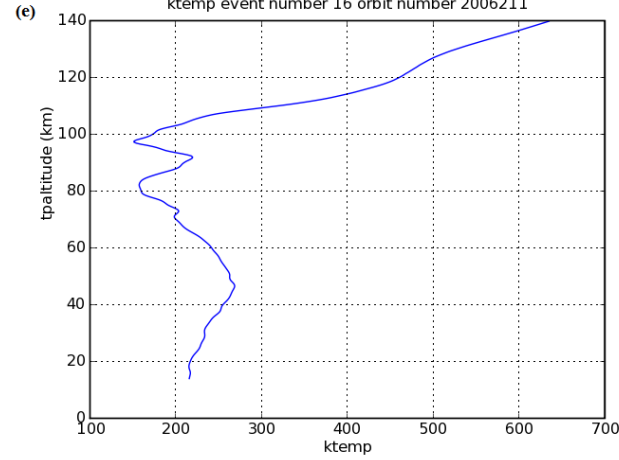
8-7-2005



25-10-2005



23-7-2006



23-8-2006

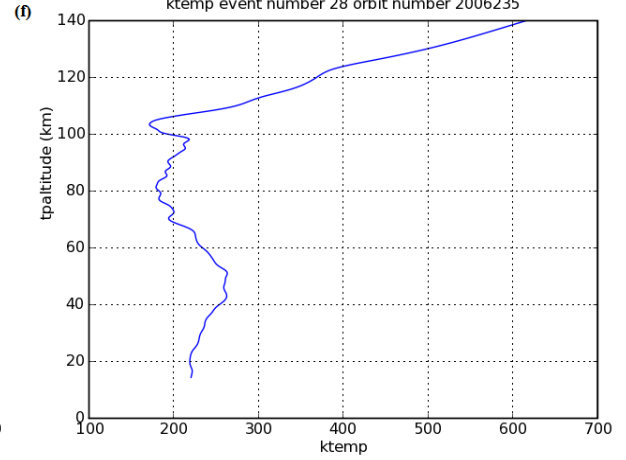


Figure 5